

RECONSTRUCTION OF DYNAMICAL SYSTEMS FROM DATA WITHOUT TIME LABELS

ZHIJUN ZENG*, PIPI HU †, CHENGLONG BAO ‡, YI ZHU §, AND ZUOQIANG SHI ¶

Abstract. In this paper, we study the method to reconstruct dynamical systems from data without time labels. Data without time labels appear in many applications, such as molecular dynamics, single-cell RNA sequencing, etc. Reconstruction of dynamical system from time sequence data has been studied extensively. However, these methods do not apply if time labels are unknown. Without time labels, sequence data becomes distribution data. Based on this observation, we propose to treat the data as samples from a probability distribution and try to reconstruct the underlying dynamical system by minimizing the distribution loss, sliced Wasserstein distance more specifically. Extensive experiment results demonstrate the effectiveness of the proposed method.

Key words. Dynamical system recovery; Data without time label; Wasserstein distance

AMS subject classifications. 65L09, 34A55, 93B30

1. Introduction. Dynamical models are crucial for enhancing our comprehension of the natural world. It is a common situation that high-dimensional observations are generated by hidden dynamical systems operating within a low-dimensional space, a concept related to the manifold hypothesis.[10]. Reconstructing evolutionary trajectory, and even more challenging, unveiling hidden dynamics from data without time labels, provides vital insights for deducing underlying mechanisms across various scientific disciplines.

System Identification. In traditional system identification problem, the observations are trajectory data with time labels $\{(t_i, \mathbf{x}_i)\}_{i=1}^n$ and the target is to determine the representation dynamic $\mathbf{x}_\theta(t)$ or the differential form $\frac{d\mathbf{x}}{dt} = \mathbf{f}(\mathbf{x}, \boldsymbol{\theta})$ that approximates the trajectory. Conventionally, the standard forward solver-based nonlinear least squares(FSNLS) approach can be distilled into four steps: (1) proposing an initial set of parameters, (2) solving the forward process on the collocation points utilizing a numerical solver, (3) comparing the generated solution with observational samples and updating the parameters, and (4) iterating steps (2) and (3) until the convergence criteria are satisfied. As a well-established topic, [1] and [18] provide a comprehensive overview of extant results. A direct comparison of evolving trajectory of differential equations forces the simulation error descent within a supervised framework, but is challenged by many numerical issue, such as non-convexity, high sensitivity to initial guess and computational cost. On the other hand, the Neural Ordinary Differential Equation (ODE) approach and its derivatives combine the forward solver-based least square method with overparametrized neural network ansatz of forcing term and bring a powerful tool for inferring the dynamics in physical systems[34][6][22][14].

Contrasting with the forward solver-based methodology, an alternative approach, known as the sparse identification of nonlinear dynamics (SINDy)[4][3], avoids forward computation by evaluating the nonlinear candidate basis functions on the given

* Department of Mathematical Sciences, Tsinghua University. zengzj22@mails.tsinghua.edu.cn.

†Microsoft Research AI4Science pisquare@microsoft.com

‡Yau Mathematical Sciences Center, Tsinghua University and Yanqi Lake Beijing Institute of Mathematical Sciences and Applications. clbao@tsinghua.edu.cn

§Yau Mathematical Sciences Center, Tsinghua University and Yanqi Lake Beijing Institute of Mathematical Sciences and Applications. yizhu@tsinghua.edu.cn

¶Yau Mathematical Sciences Center, Tsinghua University and Yanqi Lake Beijing Institute of Mathematical Sciences and Applications. zqshi@tsinghua.edu.cn

dataset and estimates the system parameters using sparse regression methods. Numerous subsequent studies have augmented the performance of this foundational concept by refining the estimation of differentiation and least square [20][15][9].

Extract dynamics from unlabelled data. In contrast to time series data, it is frequently the case that the observed datasets consist solely of point clouds enriched with feature information, while missing parametrization such as time labels. Assuming that these observational datasets are generated from an underlying dynamical system, the reconstruction of the system as well as missing parametrization necessitates supplementary information, where in this article we posit the utilization of parameter distribution information for this purpose. Rigorous mathematical definition of this problem will be presented in the subsequent Section 2. As a real-world example, Single-cell RNA sequencing (scRNA-seq) is closely aligned with the setting of unlabelled data. Within the realm of Genomics, scRNA-seq datasets provide transcriptomic profiles for thousands of individual cells in the form of high-dimensional point clouds, wherein each element represents the gene expression for a specific cell. Given the presence of the cell life cycle, these datasets can be regarded as random samples drawn from a finite length time trajectory $[0, T]$. The Trajectory Inference problem in scRNA-seq entails inferring pseudotemporal orderings or assigning cells with a continuous variable (time) as label [24]. In TI’s setting, the observations are assumed to be sampled i.i.d from the distribution of the cell expression, which can be perceived as a trajectory with time instants sampled from an uniform distribution.

Reconstructing the missing temporal labels, one of our primary objectives, can be regarded as extracting a one-dimensional parametrization of a manifold. This process is intimately connected to manifold learning techniques, which has been widely employed to derive pseudo-temporal orderings of data points along with clustering techniques and topological constraints in the early stage of TI research. One idea is to require the representation to preserve global structures, such as multi-dimensional scaling (MDS) and its variants like isometric mapping (ISOMAP) [26], uniform manifold approximation and projection (UMAP) [19], etc. One can also seek to find subspace which preserve local structure, among them the representative works are local linear embedding (LLE) [23], Laplacian eigenmaps (LE) [2], t-distributed stochastic neighbor embedding (t-SNE) [28], etc. Contemporary approaches utilize graph-based method [12][31] and deep learning method [7] to obviate the necessity for a priori knowledge of the network topology and enhance robustness. However, to extract the hidden dynamics, a different observation distribution condition leads to profoundly divergent dynamics, which until now hasn’t been solved.

From the perspective of generative model, the driven dynamics serve as an transport map between observation time to high-dimensional data points. In this field, many forms of model try to extract latent representation and transport map to generate real-world high dimensional data, such as variational auto-encoder [16], GANs [11], normalizing flows [17], diffusion models [25][27]. However, generative model is usually considered to be good at modelling high dimensional complex distribution with redundant latent dimension but sometimes failed in parametrizing manifold data, which is often referred to as Mode Collapse. [33]

Contribution. To resolve this issue, we devise a framework for the automated reconstruction of time labels and the inference of the associated hidden dynamics of observed trajectories. Observing that the conventional FSNLS framework is plagued by non-convexity and numerical issues like computational cost and instability, we directly approximate the solution of the hidden dynamics employing a surrogate model

and estimate its form utilizing an alternating direction optimization technique. The estimated parameters are fine-tuned through a forward solver-based estimation algorithm, while the time labels are obtained by projecting the observation particle onto the simulated solution curve. Main advantages of our work include:

- (1) **Accurate system identification:** Obtaining an accurate preliminary approximation, our approach utilizes a forward-based estimator to obtain refined estimation of parameters, crucial for systems exhibiting sensitivity to its parameters. We directly compare the generated solution with the observed trajectory to ascertain the inferred dynamics exhibit sufficient proximity in the forward procession. We demonstrate this capability in intricate dynamic systems such as Lorenz63 and Lotka-Volterra.
- (2) **Efficient reconstruction of the time labels:** Instead of learning the parametrization of ODE systems, we directly approximate the solution function to avoid performing forward solving and thus gain high efficiency. Using the alternating direction optimization, we not only obtain an accurate solution function but also receive relatively close guess of parameters in ODE system even for some with complex structures.
- (3) **Applicable to arbitrary distribution:** The observation distribution has great impact on the hidden parameters of trajectory. Our method put the observation distribution into consideration to infer parameters in more general cases compare to other manifold representation learning work. Therefore, we are able to reconstruct velocity and time labels in the right scale.

The organization of the paper is as follows: In Section 2, we explicate the mathematical formulation of our problem. Subsequently, Section 3 explains the process in which our method estimates the parameter of the hidden dynamics and reconstructs the time label, wherein we partition the algorithm into two distinct phases. Main results and some discussions are summarized in Section 4, followed by the conclusion of our research and an exploration of prospective avenues in Section 5.

2. Problem Statement. Consider a general case that we collect data of L different trajectories from an unknown dynamical system but different initial states. Indeed, for the l -th trajectory, the observation instants $t^l \in \mathbb{R}^1$ is a random variable with a known distribution \mathbb{P}_l whose probability density function is $p_l : \mathbb{R}^1 \rightarrow \mathbb{R}^1$ that supported on $[t_0^l, t_0^l + T^l]$ (such as uniform distribution $U(t_0^l, t_0^l + T^l)$). Therefore, the observation samples $\mathbf{x}_{ob}^l \in \mathbb{R}^d$ is a random vector which transforms t^l by the dynamics $\mathbf{x}^l(\cdot)$ with measurement noise ϵ

$$(2.1) \quad \mathbf{x}_{ob}^l = \mathbf{x}^l(t^l) + \epsilon \quad \text{where} \quad t^l \sim \mathbb{P}_l(t^l).$$

Here we assume that the dynamical system $\mathbf{x}^l(t)$ evolves according to an autonomous ordinary differential equation with different initial condition

$$(2.2) \quad \begin{cases} \frac{d\mathbf{x}^l}{dt} = \mathbf{f}(\mathbf{x}^l, \boldsymbol{\theta}), t \in [t_0^l, t_0^l + T^l] \\ \mathbf{x}^l(t_0^l) = (\mathbf{x}_1^l(t_0), \dots, \mathbf{x}_d^l(t_0))^T \in \mathbb{R}^d. \end{cases}$$

The general goal is to find an approximating dynamical system, i.e. the forcing term $\mathbf{f}(\mathbf{x}, \tilde{\boldsymbol{\theta}})$ such that the L random vectors $\{\mathbf{x}_{\tilde{\boldsymbol{\theta}}}^l(t^l)\}_{l=1}^L$ generated by the dynamical system (2.2) with $t^l \sim \mathbb{P}_l$ approach to \mathbf{x}_{ob}^l in the sense of distribution. To this end,

we formulate our goal into a minimization problem

$$(2.3) \quad \begin{aligned} \min_{\tilde{\theta} \in \Theta} \quad & \sum_{l=1}^L W_2^2(\mathbb{P}_{\mathbf{x}_{\tilde{\theta}}^l(t^l)}, \mathbb{P}_{\mathbf{x}_{ob}^l}) + \lambda \|\tilde{\theta}\|_0 \\ \text{s.t.} \quad & \begin{cases} \frac{d\mathbf{x}_{\tilde{\theta}}^l}{dt}(t) = \mathbf{f}(\mathbf{x}_{\tilde{\theta}}^l, \tilde{\theta}), t \in [t_0^l, t_0^l + T^l] \\ \mathbf{x}_{\tilde{\theta}}^l(t_0^l) = \mathbf{x}^l(t_0^l) \\ t_l \sim \mathbb{P}_l \end{cases}, \end{aligned}$$

where Θ denotes the parametric space which $\tilde{\theta}$ belongs to, W_2^2 denotes the quadratic Wasserstein distance, $\mathbb{P}_{\mathbf{x}_{\tilde{\theta}}^l(t^l)}$ denotes the distribution of $\mathbf{x}_{\tilde{\theta}}^l(t^l)$, $t^l \sim \mathbb{P}_l$ and $\mathbb{P}_{\mathbf{x}_{ob}^l}$ denotes the distribution of the l -th trajectory's observation \mathbf{x}_{ob}^l . Here we assume that the initial condition of each trajectory $\mathbf{x}^l(t_0^l)$ is known.

In the real setting, let $\mathbb{X}^l = \{\mathbf{x}_1^l, \mathbf{x}_2^l, \dots, \mathbf{x}_n^l\}$ be discrete-time observed data of the l -th trajectory. The data is generated from the process 2.2 at n time points $\mathbf{t}^l = \{t_1^l, \dots, t_n^l\}$ sampled i.i.d from \mathbb{P}_l . We further hope to reconstruct the unknown time labels \mathbf{t}^l given the observed data \mathbb{X}^l and the identified dynamical system $\mathbf{x}_{\tilde{\theta}}^l(\cdot)$.

To analyze the uniqueness of the inference problem of single trajectory case, we here consider all C^1 curve in d -dimensional cube $[0, 1]^d$ as $\mathcal{C} = \{r | r : [0, T] \rightarrow [0, 1]^d \text{ is } C^1 \text{ for some } T > 0, \|\frac{dr}{dt}\|_2 > 0, \forall t\}$.

We state that the C^1 trajectory is uniquely determined by the data distribution, the known distribution of observation time instants and initial condition. The proof is provided in Appendix A

THEOREM 2.1. *Given the observation distribution $\mathbf{t} \in \mathcal{T}$ with CDF $P(\cdot) \in \mathcal{P}$, the observed random vector \mathbf{x}_{ob} and the initial point \mathbf{x}_0 , the smooth dynamical system $\mathbf{x}(\cdot) \in \mathcal{C}$ that transform \mathbf{t} to \mathbf{x}_{ob} is unique.*

3. Methodology. In this section, we present a two-phase learning framework to extract an determined dynamical system as the transformation of random variables from data without time labels.

In the parameter identification phase, by leveraging the sliced Wasserstein distance (SWD) and dictionary representation, we formalize the problem as an optimization task and propose the corresponding FSNLS algorithm. This algorithm solves a parameterized ODE system at the time instants sampled from the observation distribution and minimizes the SWD between the generated trajectories and the observed samples. However, it requires a good initial guess to make the algorithm stable.

Inspired by the frameworks presented in [32] and [5], we propose a deep learning-based approach that significantly accelerates the initial training phase and delivers a more accurate preliminary estimation for subsequent FSNLS correction, a stage we refer to as the distribution matching phase. In this phase, a neural network works to approximate the solution function of ODEs by iteratively minimizing a distributional distance. Concurrently, physics-informed regularization is employed to ensure the solution function's required smoothness and to provide a estimate of the hidden dynamics.

Since computational experiments reveal that short trajectories are easier to identify than lengthy and intricate ones, we initially partition the long trajectory into abbreviated segments utilizing an unsupervised clustering technique for systems exhibiting complex phase spaces.

3.1. Parameter Identification. In this subsection, we investigate the traditional approach to solve the problem (2.3). Forward-solver-based nonlinear least

square(FSNLS), as delineated in Section 1, recovers the unknown forcing term utilizing an shooting and estimating pipeline under certain representation. In this article, we adopt the dictionary representation for the unknown term and develop practical algorithm to estimate its coefficients. Indeed, let

$$\phi(\mathbf{x}) = [\mathbf{f}_1(\mathbf{x}), \mathbf{f}_2(\mathbf{x}), \dots, \mathbf{f}_s(\mathbf{x})].$$

denotes the dictionary with s candidate functions $\mathbf{f}_s : \mathbb{R}^d \rightarrow \mathbb{R}^d$, then the forcing term can be represented as the linear combination of all candidates with weight $\tilde{\boldsymbol{\theta}} \in \mathbb{R}^s$. Furthermore, we modify the original task 2.3 into a computable problem by introducing the sliced Wasserstein distance(SWD)

$$(3.1) \quad \begin{aligned} \min_{\tilde{\boldsymbol{\theta}} \in \Theta} \quad & \sum_{l=1}^L SW_2^2(\mathbb{P}_{\mathbf{x}_{\tilde{\boldsymbol{\theta}}}^l(t^l)}, \mathbb{P}_{\mathbf{x}_{ob}^l}) + \lambda \|\tilde{\boldsymbol{\theta}}\|_0 \\ \text{s.t.} \quad & \begin{cases} \frac{d\mathbf{x}_{\tilde{\boldsymbol{\theta}}}^l}{dt}(t) = \phi(\mathbf{x}_{\tilde{\boldsymbol{\theta}}}^l)\tilde{\boldsymbol{\theta}}, t \in [t_0^l, t_0^l + T^l] \\ \mathbf{x}_{\tilde{\boldsymbol{\theta}}}^l(t_0^l) = \mathbf{x}^l(t_0^l) \\ t_l \sim \mathbb{P}_l \end{cases}, \end{aligned}$$

where SW_2 denotes the sliced Wasserstein distance, a computationally efficient metric between two probability measures

$$(3.2) \quad SW_2(\mu, \nu) = \mathbb{E}_{\omega \sim \mathcal{U}(\mathbb{R}^{d-1})} (W_2^2(\omega_{\#}\mu, \omega_{\#}\nu))^{\frac{1}{2}}$$

where $\omega_{\#}$ denotes the pushforwards of the projection $\mathbf{x} \in \mathbb{R}^d \rightarrow \langle \mathbf{x}, \omega \rangle$.

Given an estimated $\tilde{\boldsymbol{\theta}}$, we approximate the target function by discretizing the ODEs on sampled time instants. Indeed, for the l -th trajectory, we first sample $\{t_i^l\}_{i=1}^B$ i.i.d from \mathbb{P}_l and $\{\mathbf{x}_{ob,i}^l\}_{i=1}^B$ uniformly from \mathbb{X}_l . Then we can obtain samples of $\mathbb{P}_{\mathbf{x}_{\tilde{\boldsymbol{\theta}}}^l(t^l)}$ by solving the ODEs on the time instants

$$(3.3) \quad \mathbf{x}_{\tilde{\boldsymbol{\theta}}}^l(t_i^l) = \text{ODESolve}(\phi(\mathbf{x}_{\tilde{\boldsymbol{\theta}}}^l)\tilde{\boldsymbol{\theta}}, \mathbf{x}(t_0^l), [t_0^l, t_0^l + T^l]).$$

Note that for multi-trajectory observation, the sampling process of each trajectory can be parallelly computed. Utilizing samples from two distributions $\mathbb{P}_{\mathbf{x}_{\tilde{\boldsymbol{\theta}}}^l(t^l)}$ and $\mathbb{P}_{\mathbf{x}_{ob}^l}$, we finally approximate the distributional loss of each piece by Monte-Carlo approximation

$$(3.4) \quad L_l = SW_2^2(\mathbb{P}_{\mathbf{x}_{\tilde{\boldsymbol{\theta}}}^l(t^l)}, \mathbb{P}_{\mathbf{x}_{ob}^l}) \approx \frac{1}{M} \sum_{j=1}^M \left(W_2^2 \left(\omega_{\#}^j \{ \mathbf{x}_{\tilde{\boldsymbol{\theta}}}^l(t_i^l) \}_{i=1}^B, \omega_{\#}^j \{ \mathbf{x}_{ob,i}^l \}_{i=1}^B \right) \right)^{\frac{1}{2}},$$

where $\omega^j \sim \mathcal{U}(\mathbb{R}^{d-1})$.

On the other hand, we introduce the term $\|\tilde{\boldsymbol{\theta}}\|_0$ to account for the sparsity of the dictionary representation. We argue that the principle of sparsity in modeling is fundamentally rooted in the Occam's Razor principle. This principle suggests that, in explaining the latent dynamics within data, the primary goal should be to select the simplest possible model. Favoring models with the fewest non-zero coefficients not only enhances the interpretability of the model but also mitigates the risk of overfitting the data. However, the optimization task is highly intractable since the l_0 regularization makes this problem np-hard. To address this, we simply eliminate terms with coefficients below a predetermined threshold following a post-warm-up training

Algorithm 3.1 Parameter identification phase algorithm

Input: $\{\mathbb{X}_l\}_{l=1}^L, \{\mathbf{x}^l(t_0^l)\}_{l=1}^L, \{\mathbb{P}_l\}_{l=1}^L, Iter, Batch, \tilde{\boldsymbol{\theta}}, \hat{\theta}, Iter_1$
for $it = 1 : Iter$ **do**
 $L_{total} = 0$
for $l = 1 : L$ **do**
Sample $\{t_i^l\}_{i=1}^B \sim \mathbb{P}_l$
Uniformly sample $\{\mathbf{x}_{ob,i}^l\}_{i=1}^B$ from \mathbb{X}_l
Obtain $\{\mathbf{x}_{\tilde{\boldsymbol{\theta}}}^l(t_i^l)\}_{i=1}^B$ by solving IVP with initial condition $\mathbf{x}^l(t_0^l)$
Compute SWD loss L_l by 3.4, $L_{total} = L_{total} + L_l$
end for
Update $\tilde{\boldsymbol{\theta}}$ by gradient descent of L_{total}
if $k > Iter_1$ **then**
Eliminate $\tilde{\boldsymbol{\theta}}_j$ if $|\tilde{\boldsymbol{\theta}}_j| > \hat{\theta}$
end if
end for
return $\tilde{\boldsymbol{\theta}}$

phase. We present in Algorithm 3.1 the summary of procedure in the parameter identification phase.

Leveraging the identified parameters $\tilde{\boldsymbol{\theta}}$ we recovery the observation time of each data point by solving the IVP at a dense uniform grid $\{\hat{t}_i^l\}_{i=1} \subset [t_0^l, t_0^l + T_l]$ for trajectory l . The unlabeled observation \mathbb{X}_l are then projected onto the obtained labeled trajectory $\mathbf{x}_{\tilde{\boldsymbol{\theta}}}^l(t_i^l) =$ by solving an optimization problem

$$(3.5) \quad \min_{\{t_j^l\}_{j=1}^n \subset \{\hat{t}_i^l\}_{i=1}^M} \sum_{j=1}^n \|\mathbf{x}_j^l - \mathbf{x}_{\tilde{\boldsymbol{\theta}}}^l(t_j^l)\|_2^2.$$

However, we observe that many limiting factors exist with the practical use of the FSNLS method in reconstructing dynamical systems with complicated observation. Indeed, an randomly initialized or under-fitting weight $\tilde{\boldsymbol{\theta}}$ could lead to numerical explosion in long-time integration for even with simple dictionary. Besides, the sampled observation time instants together form a non-uniform time grid, which further increases numerical error. To take this into account, one may solve the ODEs utilizing higher order scheme, which will introduce significant computational expense since the back-propagation through an long recurrent trajectory is costly. Apart from this, the optimization problem 3.1 itself is non-convex for some complicated observation and large dictionary. This will lead to the optimization process converging to local minima for the randomly initialized parameters. We illustrative experiment of these phenomenas in AppendixB.

3.2. Distribution Matching. To address the aforementioned problem, we will introduce a novel method to fast estimate the weight $\tilde{\boldsymbol{\theta}}$ leveraging a deep neural networks surrogate model for the ODEs' solution $\mathbf{x}_{\boldsymbol{\theta}}^l(t)$. Here DNNs can be viewed as a generator, i.e. a multi-dimensional transformation from the prior distribution (observation distribution) to the solution distribution in phase space.

Specifically, we employ L separate DNNs $\mathbf{x}_{\psi}^l(\cdot)$ to approximate the solution function of L observation trajectories since their initial conditions are different. Utilizing the surrogate models, we modify 3.1 to approximate the solution via distributional

loss

$$(3.6) \quad \min_{\psi \in \Psi} \sum_{l=1}^L \left[SW_2^2(\mathbb{P}_{\mathbf{x}_{\psi}^l(t^l)}, \mathbb{P}_{\mathbf{x}_{ob}^l}) + \lambda_{\text{init}} \|\mathbf{x}_{\psi}^l(t_0^l) - \mathbf{x}^l(t_0^l)\|_2 + \lambda_{\text{reg}} \text{Reg}(\mathbf{x}_{\psi}^l) \right]$$

where $\text{Reg}(\cdot)$ is the regularization term to avoid overfitting. In this target, the expensive process of numerical integration is substituted with the direct evaluation of DNNs, enabling the rapid training to obtain a set of approximated solution functions. Using the learned surrogate models, one can extract the weight of dictionary representation using SINDy type methods[4].

To solve the problem (3.6), we optimize the parameters iteratively with single trajectory information each step:

1. Uniformly sample $\{\mathbf{x}_{ob,i}^l\}_{i=1}^B$ from \mathbb{X}_l and sample $\{t_i^l\}_{i=1}^B$ from \mathbb{P}_l .
2. Calculate the solution $\{\mathbf{x}_{\psi}(t_i^l)\}_{i=1}^B$ of each time instant.
3. Approximate the target function of each piece by

$$L_l = \frac{1}{M} \sum_{j=1}^M \left(W_2^2 \left(\omega_{\#}^j \{\mathbf{x}_{\psi}(t_i^l)\}_{i=1}^B, \omega_{\#}^j \{\mathbf{x}_{ob,i}^l\}_{i=1}^B \right) \right)^{\frac{1}{2}} + \lambda_{\text{in}} \|\mathbf{x}_{\psi}(t_0^l) - \mathbf{x}^l(t_0^l)\|_2^2 + \lambda_{\text{reg}} \text{Reg}(\mathbf{x}_{\psi})$$

where $\omega^j \sim \mathcal{U}(\mathbb{R}^{d-1})$.

4. Update the parameter $\tilde{\boldsymbol{\theta}}$.

Numerous options exist for the regularization term. Drawing inspiration from [5], we devise the regularization term as the residual of ODEs to combine the distribution matching and parameter identification cohesively, which we called it as Physics-informed regularization

$$(3.7) \quad \text{Reg}_{\tilde{\boldsymbol{\theta}}}(\mathbf{x}_{\psi}) = \int_{t_0^l}^{t_0^l + T^l} \|\phi(\mathbf{x}_{\psi}^l(t))\tilde{\boldsymbol{\theta}} - \dot{\mathbf{x}}_{\psi}^l(t)\|_2 dt + \lambda_{\text{sparse}} \|\tilde{\boldsymbol{\theta}}\|_0,$$

where the time derivative $\dot{\mathbf{x}}_{\psi}^l(t)$ is calculated by automatic differentiation and the integration of Physics-informed regularization is calculated on a time grid of $[t_0^l, t_0^l + T^l]$ with uniform step size. This transforms Problem 3.6 into a joint optimization problem involving the neural network parameters ψ and the weights $\tilde{\boldsymbol{\theta}}$. Even with the $\|\tilde{\boldsymbol{\theta}}\|_0$ term excluded, this optimization problem remains challenging due to the integration of various tasks. To ensure training stability of $\tilde{\boldsymbol{\theta}}$ and ψ , the Alternating Direction Optimization(ADO) is introduced which freezes $\tilde{\boldsymbol{\theta}}$ while training ψ and updates $\tilde{\boldsymbol{\theta}}$ every a few iterations. Indeed, given the estimated solution function \mathbf{x}_{ψ} in the training stage, we update $\tilde{\boldsymbol{\theta}}$ by utilizing sequential threshold ridge regression (STRidge) to solve the following least square problem

$$(3.8) \quad \min_{\tilde{\boldsymbol{\theta}}} \|\phi(\mathbf{X}_{\psi})\tilde{\boldsymbol{\theta}} - \dot{\mathbf{X}}_{\psi}\|_2^2 + \lambda_{\text{sparse}} \|\tilde{\boldsymbol{\theta}}\|_0.$$

where we evaluate the approximate solutions on equidistant time grid and concat them in $\mathbf{X}_{\psi} = [\mathbf{x}_{\psi}^1(t_0^1), \dots, \mathbf{x}_{\psi}^1(t_0^1 + T^1), \dots, \mathbf{x}_{\psi}^L(t_0^L), \dots, \mathbf{x}_{\psi}^L(t_0^L + T^L)]^{\top}$, and $\dot{\mathbf{X}}_{\psi}$ denotes the time derivative of \mathbf{X}_{ψ} evaluated by auto-grad. STRidge is a hybrid algorithm that combines the regularization strength of Ridge Regression with a sparsity-promoting sequential thresholding technique. By iteratively applying a threshold to set small coefficients to zero after each Ridge Regression step, STRidge aims to identify the most significant predictors in a dataset, thereby creating sparse models.

Algorithm 3.2 Distribution matching phase algorithm

Input: $\{\mathbb{X}_l\}_{l=1}^L, \{(t_0^l, T_l, \mathbf{x}^l(t_0^l))\}_{l=1}^L, \{\mathbb{P}_l\}_{l=1}^L, Iter, Iter_{phase1}, Iter_{update}, Batch$
for $Iter = 1 : Iter$ **do**
 for $l = 1 : L$ **do**
 Sample $\{t_i\}_{i=1}^{Batch} \sim \mathbb{P}_l$, uniformly sample $\{\mathbf{x}_{ob,i}^l\}_{i=1}^B$ from \mathbf{X}_l
 Compute $\{\mathbf{x}_\psi(t_i)\}_{i=1}^{Batch}$
 if $Iter \leq Iter_{phase1}$ **then**
 Compute original SWD loss and update ψ
 else
 Compute Residual-regularized SWD loss and update ψ
 if $Iter \% Iter_{update} = 0$ **then**
 Update $\hat{\boldsymbol{\theta}}$ using STRidge (3.8)
 end if
 end if
 end for
end for
return $\mathbf{x}_{\hat{\boldsymbol{\theta}}}, \hat{\boldsymbol{\theta}}$

We present in Algorithm 3.2 the summary of procedure in the parameter identification phase.

This section is referred to as the distribution matching phase. In the process of solving multi-trajectory problems, we initially employ the distribution matching phase to provide preliminary estimates of the coefficients $\hat{\boldsymbol{\theta}}$. Subsequently, these coefficients are refined during the parameter identification phase.

3.3. Trajectory Segmentation. In this subsection section, we focus on the reconstruction problem of a single trajectory. As previously mentioned, learning the transformation of random variables with complex distributions, such as a single long trajectory, poses a significant challenge. In the context of our problem, a distinct property of the dataset is that it is located along a curve situated within a high-dimensional space. By leveraging the Divide and Conquer strategy, our experiments in Appendix B show that segmenting the long trajectory into short and simple pieces could alleviate the difficulty and numerical issues.

The trajectory segmentation problem can be viewed as a unsupervised clustering challenge. Conventional clustering analysis partitions the datasets into groups, ensuring elevated intra-cluster similarity and diminished inter-cluster similarity. To segment the trajectory, the similarity between particles may be associated with the Euclidean distance or the arc length. Numerous clustering techniques exist for segmenting such manifold-type data into a specified number of classes, such as Agglomerative clustering[21], DBSCAN[8] and Spectral clustering[30].

However, in the task of trajectory segmentation, the challenge lies not only in the grouping of data but also in ascertaining the initial condition and the observation distribution of each cluster. To this end, we propose an estimation pipeline to serve as a post-processing step for the clustering procedure. Initially, we partition the dataset into non-overlapping continuous trajectory segments $\{\mathbb{X}_l\}_{l=1}^L$ via unsupervised learning method and we assume that each cluster contains data points from distinct time intervals. To estimate the initial point and observation distribution, we consider the trajectory pieces contained the highest number of elements that coincide with an neighbourhood $B_r(\mathbf{x}_0)$ of the initial point \mathbf{x}_0 as the foremost trajectory. To determine

the subsequent trajectory pieces, we adopt the following rules to select the tail element of \mathbb{X}_l and the head element of next trajectory piece \mathbb{X}_{l+1} given the initial point $\mathbf{x}_{\text{Tail},l}$

$$\begin{cases} \mathbf{x}_{\text{Tail},l} &= \arg \min_{\mathbf{x} \in \mathbb{X}_l \setminus B_r(\mathbf{x}_{\text{Head},l})} \#\{\mathbf{y} | \mathbf{y} \in \mathbb{X}_l \cap B_r(\mathbf{x})\} \\ \mathbf{x}_{\text{Head},l+1} &= \arg \max_{\mathbf{x} \in \mathbb{X}_{l+1}} \#\{\mathbf{y} | \mathbf{y} \in \mathbb{X}_l \cap B_r(\mathbf{x})\} \end{cases} .$$

where $\#$ denotes the element number of a set, and the next trajectory piece is selected as the one that intersects the most with $B_r(\mathbf{x}_{\text{Tail},l})$.

Finally, we use the two-side truncated distribution to estimate the observation distribution of each trajectory piece. Suppose a trajectory piece contains n_l elements and the initial time is t_0^l , then the restricted observing instants \mathbf{t}_l as a random variable is

$$\mathbf{t}_l = \mathbf{t} \mathbb{I}_{t_0^l < t < P^{-1}(P(t_0^l) + \frac{n_l}{n})} \sim \mathbb{P}_l$$

where P is the probability distribution function of \mathbb{P} and $\mathbf{t} \sim \mathbb{P}$. That is, we employ the frequency to approximate the proportional length of a trajectory segment. Undoubtedly, the segmentation process may encounter failure owing to the overlapping and twining conformation of trajectory, which we defer to further work. Empirically, we discern that Agglomerative clustering exhibits heightened robustness against noise, and as such, our experimentation is based on this clustering technique. We encapsulate the trajectory segmentation methodology in Algorithm 3.3 and illustrate the segmentation results for several systems in 1.

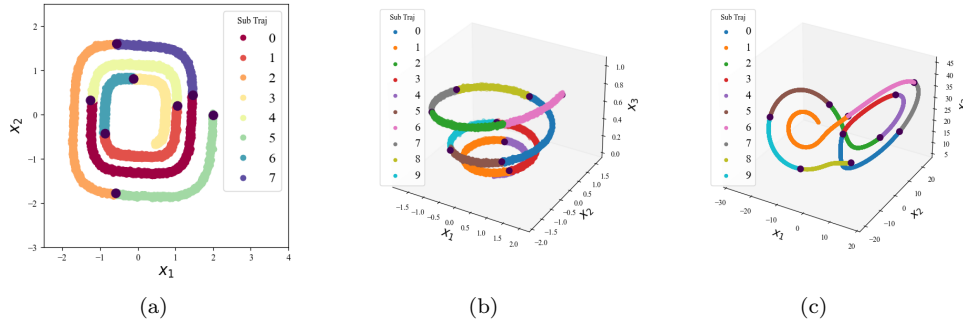


FIG. 1. Segmentation result of illustrative problem:(a) is the 8 piece cluster result of Cubic2D ODE system initiate at $(2, 0)$ with $T = 10$;(b) is the 10 piece cluster result of Linear3D ODE system initiate at $(2, 0, -1)$ with $T = 10$;(c) is the 10 piece cluster result of Lorenz ODE system initiate at $(10, 20, -10)$ with $T = 3$.

4. Experiments. In this section, we shall employ our methodology to the elementary demonstrative systems delineated in [4], the Lorenz equations and Duffing equations in the chaotic regime, the Lotka-Volterra systems in high dimensional regime, the pendulum equations in non-polynomial regime. This article focuses on the reconstruction problem of single long trajectory, which has intrinsic difficulties. Further more, we accurately divide it into multiple sub-trajectories for comparison. In the following, we will evaluate the precision, the robustness and the efficacy for non-uniform observation distribution of our approach and highlight its advantages.

Algorithm 3.3 Trajectory segmentation algorithm

Input: $\mathbb{X}, \mathbb{P}, \mathbf{x}(t_0), T, L$
 $\{\mathbb{X}_l\}_{l=1}^L = \text{Clustering}(\mathbb{X}, L)$
for $l = 1 : L$ **do**
 $t_0^{l+1} = P^{-1}(P(t_0^l) + \frac{n_l}{n})$
Determine $\mathbf{x}(t_0^{l+1}) = \mathbf{x}_{\text{Head}, l+1}$ by (3.3)
 $t_l = \mathbf{t}_{t_0^l < t < P^{-1}(P(t_0^l) + \frac{n_l}{n})} \sim \mathbb{P}_l, T_l = t_0^{l+1} - t_0^l$
end for
return $\{(\mathbb{X}_l, t_0^l, T^l, \mathbf{x}(t_0^l), \mathbb{P}_l)\}_{l=1}^L$

4.1. Numerical setups and performance metrics. In our experiment, all observation datasets are generated utilizing LSODA method in [29] while the inferred trajectories are computed employing the RK4 scheme to achieve an equilibrium between computational expense and precision. For examples with uniform distribution of observation instants, we employ 50,000 temporal instants for dataset generation and a discrete set of 2000 timepoints with uniform stepsize $\{t_i^*\}_{i=0}^{2000}$ is used to assess the error of the learned dynamics. Specifically, to evaluate the performance, we record the Mean Absolute Error(MAE) of every record timepoint $\{\mathbf{x}_{\tilde{\theta}}(t_i^*)\}_{i=1}^{2000}$ as a direct evaluation metric for reconstructing dynamics. To compute the MAE for the identified ODE system, we partition the uniform temporal grid into short intervals according to the estimated time length of each cluster and compute the solution of each short trajectories using the estimated initial points. Subsequently, we combine these solution trajectories to acquire $\{\mathbf{x}_{\tilde{\theta}}(t_i^*)\}_{i=1}^{2000}$. The RMAE of solution is computed by

$$RMAE = \frac{\sum_{i=1}^{2000} |\mathbf{x}_{\tilde{\theta}}(t_i^*) - \mathbf{x}(t_i^*)|}{\sum_{i=1}^{2000} |\mathbf{x}(t_i^*)|}$$

For parameter identification, we use the relative mean absolute error(RMAE)

$$E_{para} = \frac{\|\tilde{\theta} - \theta\|_1}{\|\theta\|_1}$$

where $\tilde{\theta}$ is the estimated parameters of the dynamical system and θ is the ground truth. Regarding the reconstruction of time label, we evaluate RMAE of the reconstructed time labels with ground truth

$$E_{time} = \frac{\sum_{i=1}^n |\hat{t}_i - t_i|}{\sum_{i=1}^n |t_i|}$$

The surrogate model in our experiment is a 5-layer MLP with 500 neurons in each layer and SiLU activation function. And we choose AdamW as the optimizer for both phases. All the experiment were done on the Nvidia RTX3090 and Intel Xeon Gold 6130 with 40G RAM.

4.2. Simple illustrative systems. We here apply the reconstruction algorithm to some simple systems with the following form

$$\begin{cases} \frac{d\mathbf{x}}{dt} = \mathbf{A}\mathbf{f}(\mathbf{x}), t \in [0, T] \\ \mathbf{x}(0) = (\mathbf{x}_1, \dots, \mathbf{x}_d)^\top. \end{cases}$$

1. **Linear2D equations:**The linear matrix is $A = \begin{bmatrix} -0.1 & 2 \\ -2 & -0.1 \end{bmatrix}$, the transformation is $\mathbf{f} = \mathbb{I}_d$, the initial condition is $\mathbf{x}(0) = [2, 0]$, the time length is $T = 10$.
2. **Cubic2D equations:**The linear matrix is $A = \begin{bmatrix} -0.1 & 2 \\ -2 & -0.1 \end{bmatrix}$, the transformation is $\mathbf{f} = \begin{bmatrix} x_1^3 \\ x_2^3 \end{bmatrix}$, the initial condition is $\mathbf{x}(0) = [2, 0]$, the time length is $T = 10$.
3. **Linear3D equations:**The linear matrix is $A = \begin{bmatrix} -0.1 & 2 & 0 \\ -2 & -0.1 & 0 \\ 0 & 0 & -0.3 \end{bmatrix}$, the transformation is $\mathbf{f} = \mathbb{I}_d$, the initial condition is $\mathbf{x}(0) = [2, 0, -1]$, the time length is $T = 10$.

The details of implementation parameters are delineated in table 5, and a comprehensive summary of our discoveries is provided in Fig 2. In these cases, we employ third-order complete polynomials and exponential functions as the basis for the library in both phases. Our method not only reconstructs the solution and temporal labels with exceptional precision but also accurately identifies the underlying system. Subsequent to the initial training devoid of regularization, the approximate solution derived from the neural network captures a proximate estimation of the hidden system’s trajectory. Employing the guidance of the distilled model, ADO training further refines the solution quality by harnessing a regularity ansatz from ODEs. The MAE curve and parameters’ error curve indicate that while the surrogate model adeptly approximates the solution, the inferred systems still deviate from the observed systems. This deviation is subsequently rectified by the parameter identification phase. The results imply that the identified ODE system provides comparable accuracy for temporal label reconstruction to solutions represented by neural networks. It is vital to recognize that the magnitude of the Physics-informed regularization term may exhibit variability, owing to the inherent properties of the equations themselves, necessitating a balanced approach during the training process.

Settings	$\ \mathbb{X}\ _{rms}$	RMAE	E_{para}	E_{time}	Reconstruct A
Linear2D	1.26	8.4%,1.4%	7.7%,1.9%	0.39% 0.056%	$\begin{bmatrix} -0.12 & -2.01 \\ 1.97 & -0.08 \end{bmatrix}$
Cubic2D	1.13	7.0%,0.6%	9.2%,0.8%	0.9% 0.4%	$\begin{bmatrix} -0.11 & -2.02 \\ 1.99 & -0.99 \end{bmatrix}$
Linear3D	1.31	5.7%,1.5%	6.8%,3.0%	0.53% 0.13%	$\begin{bmatrix} -0.15 & -2.01 & 0 \\ 1.97 & -0.07 & 0 \\ 0 & 0 & -2.8 \end{bmatrix}$

TABLE 1

The results of illustrative examples. For the three metrics, the first one is computed using learned neural solution in distribution matching phase while the second is computed by the solution of the learned ODE system.

4.3. Benchmark Examples. In the instances delineated below, we execute our algorithm on a selection of challenging ODE systems derived from real-world models.

1. Lorenz equations represent a early mathematical model for characterizing atmospheric turbulence. This system exhibits chaotic behavior over the long

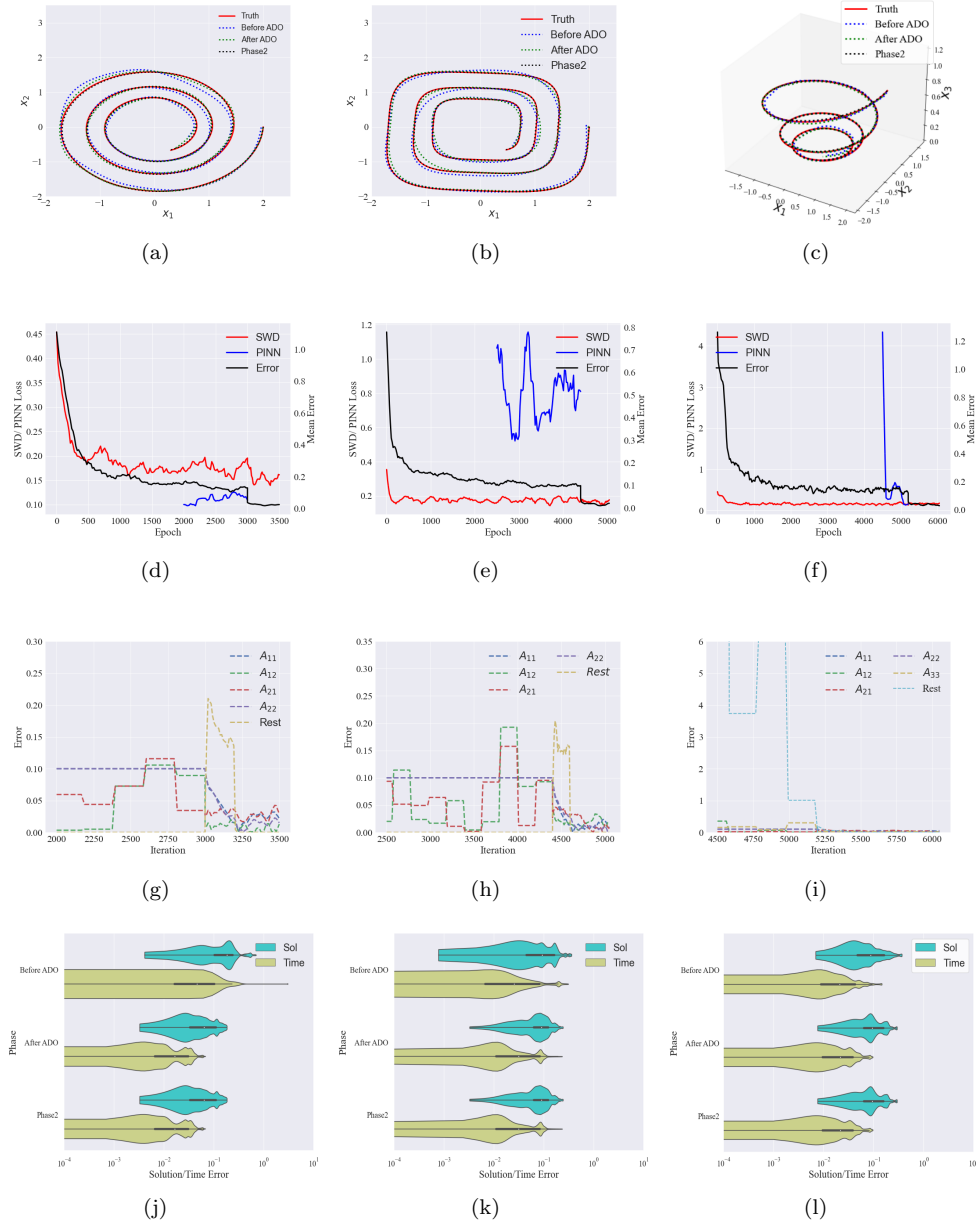


FIG. 2. Reconstruction result of illustrative system: (a)-(c) Comparison between learned curve at different stage and ground truth for all system; (d)-(f) Recorded SWD Loss, PINN Loss and Average Error for all system; (g)-(i) The error curve of parameters and the sum of unexisting terms for all system; (j)-(l) The absolute error of learned solution evaluated at uniform grid and the absolute error of reconstructed time label of the dataset.

time horizon, resulting in intricate intersecting trajectories and convoluted spiraling within the phase space

2. The Lotka-Volterra (LV) equations depict the dynamics of prey and predator

populations in natural ecosystems and have found applications in real-world systems such as disease control and pollution management. In this study, we couple two independent LV equations(LV4D) to evaluate the efficacy of our algorithm in addressing high-dimensional problems.

3. The Duffing oscillator serves as a model for specific damped and driven oscillators, demonstrating long-term chaotic behavior.

Name	ODE	Parameters
Lorenz	$\begin{cases} \frac{dx_1}{dt} = \sigma(x_2 - x_1) \\ \frac{dx_2}{dt} = x_1(\rho - x_3) - x_2 \\ \frac{dx_3}{dt} = x_1x_2 - \beta x_3 \end{cases}$	$\begin{aligned} T &= 3 \\ [\sigma, \rho, \beta] &= [10, 28, \frac{8}{3}] \\ \mathbf{x}_0 &= (10, -10, 20)^\top \end{aligned}$
Lotka-Volterra4D	$\begin{cases} \frac{dx_1}{dt} = \alpha_1x_1 - \beta_1x_1x_2 \\ \frac{dx_2}{dt} = \beta_1x_1x_2 - 2\alpha_1x_2 \\ \frac{dx_3}{dt} = \alpha_2x_3 - \beta_2x_3x_4 \\ \frac{dx_4}{dt} = \beta_2x_3x_4 - 2\alpha_2x_4 \end{cases}$	$\begin{aligned} T &= 11 \\ [\alpha_1, \alpha_2, \beta_1, \beta_2] &= [1, 1, 3, 5] \\ \mathbf{x}_0 &= (1, 2, 2, 0.5)^\top \end{aligned}$
Duffing	$\begin{cases} \frac{dx_1}{dt} = \alpha x_2 \\ \frac{dx_2}{dt} = -\gamma x_1 - \rho x_2 - \beta x_1^3 \end{cases}$	$\begin{aligned} T &= 11 \\ [\alpha, \gamma, \rho, \beta] &= [1, 0.1, 0.2, 1] \\ \mathbf{x}_0 &= (0, 2)^\top \end{aligned}$

TABLE 2
Specifications of ODE examples.

As demonstrated in Table 3 and Fig 3, our approach consistently attains precise performance across all three benchmarks, covering both chaotic and high-dimensional systems, thereby justifying versatility of our method with respect to diverse ODEs. In general, our method reconstructs the solution function with an RMAE of less than 5% and the time label with less than 0.7% after the distribution matching phase in a noise-free environment. The reconstruction quality is further enhanced during the parameter identification phase, wherein all active terms are successfully identified with an RMAE of less than 8%. We again observe that the solution and time label exhibit similar accuracy to those obtained in the distribution matching phase, thereby highlighting the efficacy of our approach. It should be noted that the reconstruction error for the solution and time label may remain high within some intervals when two trajectory pieces are close, despite the accurate identification of the model. This phenomenon can be observed in Fig 3(a)-(c) for the Lorenz system and LV4D system, whose trajectories nearly coincide at distinct intervals.

To illustrate the precision, we compare our method with Principal Curve method, a traditional manifold parametrization method in the temporal label reconstruction task. We use the index provided by Principal Curve algorithm [13] as the reconstructed time label. Indeed, we apply Principal Curve on the segmented trajectory piece and assign the estimated initial condition as the start points of each curve. The output indexes of each data point are normalized to $[T_l, T_{l+1}]$ for \mathbb{X}_l . The result shows that given the same segmentation condition, our method is more than 30 times less than traditional Principal Curve method, while the Principal Curve fails to provide inter-interval resolution of time label. This problem is partly rooted in the parametrization principle of Principal Curve algorithm. It assign index based on the Euclidean distance between points, which often mismatch the velocity of curve determined by the observation distribution.

4.4. Noisy data. Here we want to investigate the effect of noise on system identification. To this end, a noise ratio σ_{NR} is specified, and the observation data is

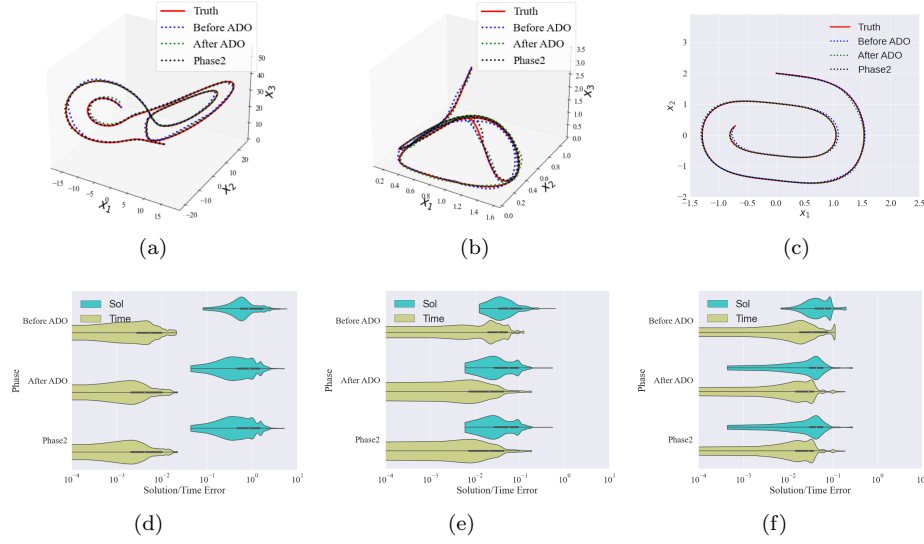


FIG. 3. Reconstructing trajectories of four systems at different training stage:(a)Lorenz system; (b)LV4D system, plot the curve of first 3 dimension;(c)Duffing system. The point-wise error of learned solution function and time label of three training stage: (a)Lorenz system; (b)LV4D system; (c)Duffing system.

Settings	$\ \hat{\mathbb{X}}\ _{rms}$	RMAE	E_{para}	E_{time}	Parameters
Lorenz	25.36	2.8%,1.5%	0.65%,0.58%	0.40%,0.10%,25.9%	$\begin{bmatrix} \sigma \\ \rho \\ \beta \end{bmatrix} = \begin{bmatrix} 9.94 \\ 27.89 \\ 2.59 \end{bmatrix}$
LV4D	1.12	4.2%,2.3%	5.6%,4.3%	0.69%,0.31%,13.0%	$\begin{bmatrix} \alpha_1 \\ \alpha_2 \\ \beta_1 \\ \beta_2 \end{bmatrix} = \begin{bmatrix} 0.97 \\ 0.98 \\ 2.93 \\ 4.65 \end{bmatrix}$
Duffing	1.17	3.88%,1.63%	8.53%,2.03%	0.30%,0.20%,19.4%	$\begin{bmatrix} \alpha \\ \gamma \\ \rho \\ \beta \end{bmatrix} = \begin{bmatrix} 0.99 \\ 0 \\ 0.21 \\ 1.06 \end{bmatrix}$

TABLE 3

The results of benchmark examples. For the three metrics, the first results is computed using learned neural solution in the distribution matching phase while the second is computed by the solution of the learned ODE system. For the E_{time} column, the third results is computed by traditional Principal Curve method. All the inactive terms in library are successfully removed during training in four experiment, so the Parameters row describes the identified systems.

blurred by

$$(4.1) \quad \hat{\mathbb{X}} = \mathbb{X} + \epsilon$$

where \mathbb{X} is the simulated noise-free observation and ϵ is the white noise with variance σ^2 , where

$$(4.2) \quad \sigma = \sigma_{NR} \times \|\mathbb{X}\|_{rms} = \sigma_{NR} \times \frac{1}{n} \sum_{i=1}^n \left(\sum_{j=1}^d \mathbf{x}_{i,j}^2 \right)^{\frac{1}{2}}$$

Besides the single trajectory setting we used above, we also present the results on observation of multiple short trajectories which can be viewed as the segmentation of a long trajectory with noise-free initial conditions. In this setting we don't do trajectory segmentation anymore. We exam the robustness again on the four benchmark systems for 1%,3% noise in single trajectory setting and 3%,5% noise in multiple trajectory setting. The three evaluation metric are summarized in Fig 4 for different setting.

As can be observed from the results, the reconstruction error of solutions and time labels generally increases as the noise level increases. The major challenge is when the noise level are large, the trajectory may overlaps and causes error in trajectory segmentation. If a cluster have two disjoint pieces with different initial point, the single trajectory condition is no longer established. When it comes to multi-trajectory problem, our method is still effective to capture the hidden dynamic precisely even with large noise level. Further more, the result shows that the non-polynomial terms introduce extra difficulty in both parameter identification and solution reconstruction for data with large noise level. However, with the help of parameter identification phase, we still obtained high-quality results.

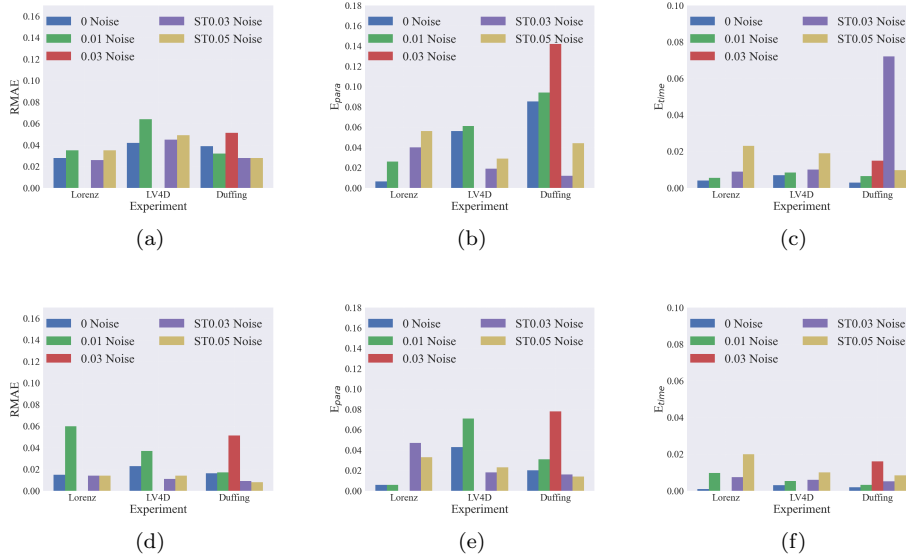


FIG. 4. Evaluation of reconstruction results from noisy data in two trajectory type and four systems. (a)-(c): The RMAE of learned solution, identified parameters and reconstructed time labels in the distribution matching phase; (d)-(f): The RMAE of learned solution, identified parameters and reconstructed time labels in the parameter identification phase. The data of Lorenz and LV4D systems for 3% noise is missing because the segmentation step failed to provide non-overlapping trajectory pieces.

4.5. General Hamiltonian system out of basis . One may have doubts about the restricted basis expansion in this framework, as the dynamical system with real-world backgrounds may not necessarily be representable by a finite set of basis functions. In this subsection, we exam the approximation capability of our method by the famous Pendulum system:

$$(4.3) \quad \begin{cases} \frac{dx_1}{dt} = \alpha x_2 \\ \frac{dx_2}{dt} = \beta \sin(x_1) \end{cases}$$

where the initial condition is $\mathbf{x}_0 = (1, 0.1)^\top$, the time length is $T = 8$ and the parameters are $[\alpha, \beta] = [1, 1]$. In this case, the Hamiltonian $H(x_1, x_2) = \frac{1}{2}x_2^2 + \cos(x_1)$ is a conserved quantity describing the total energy of a Hamiltonian system.

We first utilize our method in a larger basis

$$\phi_1 = \{Poly(3), \sin(x_1), \sin(x_2), \cos(x_1), \cos(x_2)\}$$

that contains all the existing terms in the pendulum system and a smaller 3rd order complete polynomials library $\phi_2 = \{Poly(3)\}$. Here observations with five different noise levels are considered to provide a more comprehensive view.

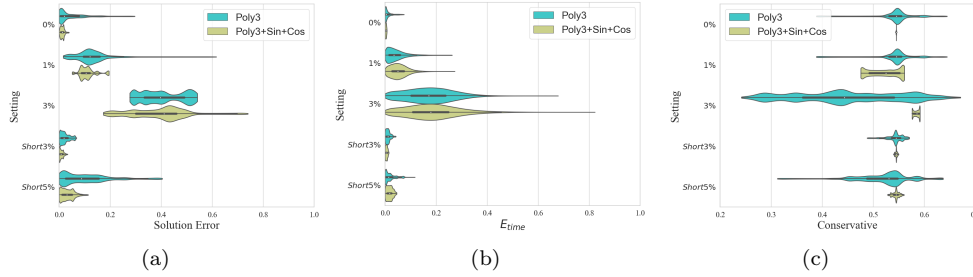


FIG. 5. Reconstruction result of Pendulum system:(a)Violin plot of absolute error of learned solution function for two basis setting in 5 different noise level;(b)Violin plot of absolute error of reconstructed time label for two basis setting in 5 different noise level;(c)Voilin plot of Hamiltonian of learned dynamical system in the parameter identification phase

The result obtained from Fig 6 demonstrates that the learned dynamical system with a general polynomial basis ϕ_2 reaches high precision in the reconstruction of solution function(1.2%RMAE for noise free setting) and time label(0.07%RMAE for noise free setting), yet slightly lower than the result of larger basis ϕ_1 (0.28%RMAE for solution function and 0.07%RMAE for time label) . However, the Hamiltonian along the learned trajectory of the restricted basis have significant larger variance than that of ϕ_1 , especially for large noise level. This is reasonable since with larger library the algorithm successfully identifies the exact components that form the conservative system, while the polynomial system does not inhibit the Hamiltonian structured, though approximated in the solution function perspective.

To investigate in the approximation capability of our method with respect to the scale of library, we approximate the source term using polynomial basis functions of 5 different orders. We compare the absolute error of solution function and the time labels for different basis in Fig6. As the order of polynomial basis from 1 increases to 4, the results obtained by our method gradually approach the ground truth, and the best learning performance is achieved when the order is 4, with 0.44% RMAE of

solution and 0.08% RMAE of time label. For $Poly(5)$ basis, the sparse regression failed to provide a convergent estimation of dynamical system on account of the increasing sensitivity of higher order parameters, while in the parameter identification phase numerical instability of forward solver causes difficulties for parameter identification since our sampled time label isn't uniform. This results in the growth of solution error and time label error.

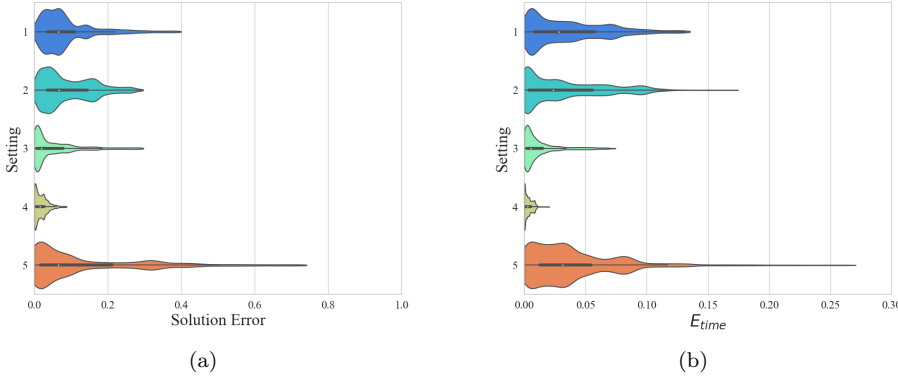


FIG. 6. Reconstruction result of Pendulum system using polynomial basis with different order:(a)Absolute error of solution with library parametrized by different order of polynomial basis;(b)Absolute error of time label with library parametrized by different order of polynomial basis.

4.6. Different observation distribution. We further investigate the robustness of our method for data with different observation distribution. Here we truncate the normal distribution $\mathcal{N}\left(\frac{T}{2}, \left(\frac{T}{3}\right)^2\right)$ in $[0, T]$ and treat it as the observation distribution. The results of four benchmark systems are shown in Fig 7 and Table 4. Overall, our method presents a stable performance w.r.t different observation distribution for reconstructing the solution and time label.

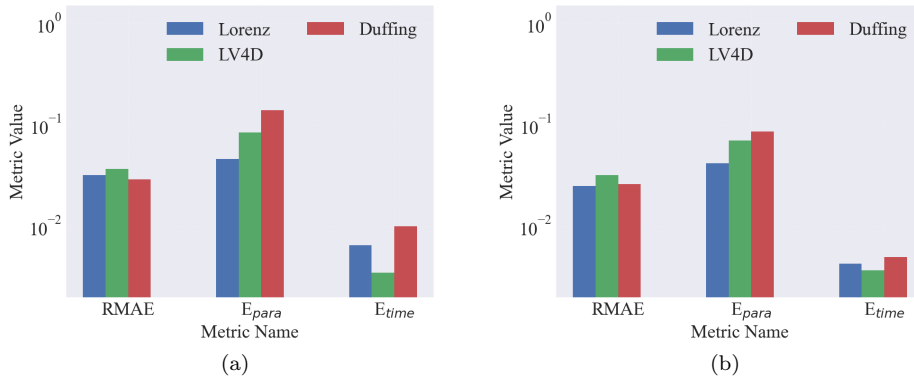


FIG. 7. Evaluation of reconstruction results from data with truncated normal distribution of observation time.(a):The evaluation metrics of reconstruction results in distribution matching phase;(b):The evaluation metrics of reconstruction results in parameter identification phase

Settings	RMAE	E_{para}	E_{time}
Lorenz	3.2%,2.5%	4.6%,4.2%	0.65%,0.43%
LV4D	3.7%,3.2%	8.4%,7.0%	0.35% 0.37%
Duffing	2.9%,2.6%	14.0%,8.6%	1.0% 0.50%

TABLE 4

The results of benchmark examples with truncated normal distribution of observation time. For the three metrics, the first one is computed using learned neural solution in distribution matching phase while the second is computed by the solution of the learned ODE system.

5. Conclusion and future work. Point cloud data lacking temporal labels is a common data type for scientific research. Unveiling the hidden dynamics and reconstructing the missing time label is helpful for understanding the physical laws behind the observation. In this study, we assume that the observation time instants is sampled from a known distribution and the observation data are generated by a ODE system with perturbation. and formulate the reconstruction into a rigorous minimization problems with respect to a continuous transformation of random variable. We perform theoretical analysis of the uniqueness of smooth transformation given the distribution of observation data and time instants under certain conditions.

In computational perspective, we propose a two-phase learning algorithm to simultaneous estimate the potential trajectory and the hidden dynamical system. In distributional matching phase, we leverage the Sliced Wasserstein Distance to construct a neural network approximation of the data trajectory and utilize Alternating Direction Optimization technique to distill sparse parameter estimation of the ODE system from a large expression library. In parameter identification phase, we adopt the Neural ODE paradigm to further refine the estimation. Based on the empirical observation that complex trajectory renders higher non-convexity and numerical issue for the learning task, we leverage the manifold hypothesis to propose a clustering based partition algorithm to transform long trajectory in to short trajectory segments before training.

On the experimental side, We demonstrate our method on a number of illustrative and complex dynamical systems exhibiting challenging characteristic (e.g., chaotic, high-dimensional, nonlinear). Results highlight that the approach is capable of uncovering the hidden dynamics of the real-world point cloud data, and reconstruct the time label in high accuracy. The proposed method maintains satisfactory robustness against different types of distribution of observation time instant (Uniform and truncated Gaussian) and high level noises when multiple short trajectories are provided, while in single trajectory setting the perturbation bring about overlapping and lead to failure in trajectory segmentation and time label reconstruction. Results show that the approximation capability is increasing as the library is enlarging, obtaining finer reconstruction of solution function and time label. However, including high-order terms in the library may introduce numerical instability in the forward computation and the regression process.

As future work, we will try the generalize our method to more challenging regime. For example, one of the important directions is to unveiling physical laws from PDE-driven or SDE-driven observation without time label. Another interesting direction which is worth exploring is to embed more statistical insight in the algorithm to enhance the robustness for highly perturbed data.

REFERENCES

- [1] H. T. BANKS AND K. KUNISCH, *Estimation Techniques for Distributed Parameter Systems*, Springer Science & Business Media, 2012.
- [2] M. BELKIN AND P. NIYOGI, *Laplacian eigenmaps for dimensionality reduction and data representation*, *Neural computation*, 15 (2003), pp. 1373–1396.
- [3] R. BELLMAN, *A new method for the identification of systems*, *Mathematical Biosciences*, 5 (1969), pp. 201–204, [https://doi.org/10.1016/0025-5564\(69\)90042-X](https://doi.org/10.1016/0025-5564(69)90042-X).
- [4] S. L. BRUNTON, J. L. PROCTOR, AND J. N. KUTZ, *Discovering governing equations from data: Sparse identification of nonlinear dynamical systems*, *Proceedings of the National Academy of Sciences*, 113 (2016), pp. 3932–3937, <https://doi.org/10.1073/pnas.1517384113>, <https://arxiv.org/abs/1509.03580>.
- [5] Z. CHEN, Y. LIU, AND H. SUN, *Physics-informed learning of governing equations from scarce data*, *Nature Communications*, 12 (2021), p. 6136, <https://doi.org/10.1038/s41467-021-26434-1>.
- [6] M. CHOI, D. FLAM-SHEPHERD, T. H. KYAW, AND A. ASPURU-GUZIĆ, *Learning quantum dynamics with latent neural ODEs*, *Physical Review A*, 105 (2022), p. 042403, <https://doi.org/10.1103/PhysRevA.105.042403>.
- [7] J.-H. DU, M. GAO, AND J. WANG, *Model-based trajectory inference for single-cell rna sequencing using deep learning with a mixture prior*, *bioRxiv : the preprint server for biology*, (2020), pp. 2020–12.
- [8] M. ESTER, H.-P. KRIEGEL, J. SANDER, X. XU, ET AL., *A density-based algorithm for discovering clusters in large spatial databases with noise*, in *Kdd*, vol. 96, 1996, pp. 226–231.
- [9] U. FASEL, J. N. KUTZ, B. W. BRUNTON, AND S. L. BRUNTON, *Ensemble-sindy: Robust sparse model discovery in the low-data, high-noise limit, with active learning and control*, *Proceedings of the Royal Society A*, 478 (2022), p. 20210904.
- [10] C. FEFFERMAN, S. MITTER, AND H. NARAYANAN, *Testing the manifold hypothesis*, *Journal of the American Mathematical Society*, 29 (2016), pp. 983–1049, <https://doi.org/10.1090/jams/852>.
- [11] I. GOODFELLOW, J. POUGET-ABADIE, M. MIRZA, B. XU, D. WARDE-FARLEY, S. OZAIR, A. COURVILLE, AND Y. BENGIO, *Generative adversarial nets*, *Advances in neural information processing systems*, 27 (2014).
- [12] D. GRÜN, A. LYUBIMOVA, L. KESTER, K. WIEBRANDS, O. BASAK, N. SASAKI, H. CLEVERS, AND A. VAN OUDENAARDEN, *Single-cell messenger RNA sequencing reveals rare intestinal cell types*, *Nature*, 525 (2015), pp. 251–255.
- [13] T. HASTIE AND W. STUETZLE, *Principal curves*, *Journal of the American statistical association*, 84 (1989), pp. 502–516.
- [14] P. HU, W. YANG, Y. ZHU, AND L. HONG, *Revealing hidden dynamics from time-series data by odenet*, *Journal of Computational Physics*, 461 (2022), p. 111203.
- [15] K. KAHAMAN, J. N. KUTZ, AND S. L. BRUNTON, *Sindy-pi: a robust algorithm for parallel implicit sparse identification of nonlinear dynamics*, *Proceedings of the Royal Society A*, 476 (2020), p. 20200279.
- [16] D. P. KINGMA AND M. WELLING, *Auto-encoding variational bayes*, *arXiv preprint arXiv:1312.6114*, (2013), <https://arxiv.org/abs/1312.6114>.
- [17] I. KOBYZEV, S. J. PRINCE, AND M. A. BRUBAKER, *Normalizing flows: An introduction and review of current methods*, *IEEE transactions on pattern analysis and machine intelligence*, 43 (2020), pp. 3964–3979.
- [18] L. LJUNG, *System identification*, in *Signal Analysis and Prediction*, Springer, 1998, pp. 163–173.
- [19] L. MCINNES, J. HEALY, N. SAUL, AND L. GROSSBERGER, *Umap: Uniform manifold approximation and projection*, *Journal of Open Source Software*, 3 (2018), p. 861.
- [20] D. A. MESSENGER AND D. M. BORTZ, *Weak sindy for partial differential equations*, *Journal of Computational Physics*, 443 (2021), p. 110525.
- [21] F. MURTAGH AND P. LEGENDRE, *Ward’s hierarchical agglomerative clustering method: Which algorithms implement Ward’s criterion?*, *Journal of classification*, 31 (2014), pp. 274–295.
- [22] M. NAKAJIMA, K. TANAKA, AND T. HASHIMOTO, *Neural Schrödinger Equation: Physical Law as Deep Neural Network*, *IEEE Transactions on Neural Networks and Learning Systems*, 33 (2022), pp. 2686–2700, <https://doi.org/10.1109/TNNLS.2021.3120472>.
- [23] S. T. ROWEIS AND L. K. SAUL, *Nonlinear dimensionality reduction by locally linear embedding*, *science*, 290 (2000), pp. 2323–2326.
- [24] W. SAELENS, R. CANNODT, H. TODOROV, AND Y. SAEYS, *A comparison of single-cell trajectory inference methods*, *Nature Biotechnology*, 37 (2019), pp. 547–554, <https://doi.org/10.1038/s41587-019-0071-9>.

- [25] Y. SONG, J. SOHL-DICKSTEIN, D. P. KINGMA, A. KUMAR, S. ERMON, AND B. POOLE, *Score-based generative modeling through stochastic differential equations*, arXiv preprint arXiv:2011.13456, (2020), <https://arxiv.org/abs/2011.13456>.
- [26] J. B. TENENBAUM, V. DE SILVA, AND J. C. LANGFORD, *A global geometric framework for nonlinear dimensionality reduction*, *science*, 290 (2000), pp. 2319–2323.
- [27] A. VAHDAT, K. KREIS, AND J. KAUTZ, *Score-based generative modeling in latent space*, *Advances in Neural Information Processing Systems*, 34 (2021), pp. 11287–11302.
- [28] L. VAN DER MAATEN AND G. HINTON, *Visualizing data using t-SNE.*, *Journal of machine learning research*, 9 (2008).
- [29] P. VIRTANEN, R. GOMMERS, T. E. OLIPHANT, M. HABERLAND, T. REDDY, D. COURNAPEAU, E. BUROVSKI, P. PETERSON, W. WECKESSER, J. BRIGHT, S. J. VAN DER WALT, M. BRETT, J. WILSON, K. J. MILLMAN, N. MAYOROV, A. R. J. NELSON, E. JONES, R. KERN, E. LARSON, C. J. CAREY, Í. POLAT, Y. FENG, E. W. MOORE, J. VANDERPLAS, D. LAXALDE, J. PERKTOLD, R. CIMRMAN, I. HENRIKSEN, E. A. QUINTERO, C. R. HARRIS, A. M. ARCHIBALD, A. H. RIBEIRO, F. PEDREGOSA, P. VAN MULBREGT, AND SCI-PY 1.0 CONTRIBUTORS, *SciPy 1.0: Fundamental algorithms for scientific computing in python*, *Nature Methods*, 17 (2020), pp. 261–272, <https://doi.org/10.1038/s41592-019-0686-2>.
- [30] U. VON LUXBURG, *A tutorial on spectral clustering*, *Statistics and computing*, 17 (2007), pp. 395–416.
- [31] F. A. WOLF, F. K. HAMEY, M. PLASS, J. SOLANA, J. S. DAHLIN, B. GÖTTGENS, N. RAJEWSKY, L. SIMON, AND F. J. THEIS, *PAGA: Graph abstraction reconciles clustering with trajectory inference through a topology preserving map of single cells*, *Genome Biology*, 20 (2019), p. 59, <https://doi.org/10.1186/s13059-019-1663-x>.
- [32] L. YANG, C. DASKALAKIS, AND G. E. KARNIADAKIS, *Generative ensemble regression: Learning particle dynamics from observations of ensembles with physics-informed deep generative models*, *SIAM Journal on Scientific Computing*, 44 (2022), pp. B80–B99.
- [33] K. ZHANG, *On Mode Collapse in Generative Adversarial Networks*, in *Artificial Neural Networks and Machine Learning – ICANN 2021*, I. Farkaš, P. Masulli, S. Otte, and S. Wermter, eds., vol. 12892, Springer International Publishing, Cham, 2021, pp. 563–574, https://doi.org/10.1007/978-3-030-86340-1_45.
- [34] Y. D. ZHONG, B. DEY, AND A. CHAKRABORTY, *Symplectic ode-net: Learning hamiltonian dynamics with control*, in *International Conference on Learning Representations*, 2019.

Appendix A. Proof of Theorem 2.1. To prove the theorem, we introduce the following assumption

ASSUMPTION A.1.

1. The probability density function (PDF) $p(t)$ of observation time instant t supports on a finite interval $[0, T]$ and satisfies $p(t) \in C([0, T])$, $p(t) > 0$ for all $t \in [0, T]$, and we denote the space of satisfied observation distribution as \mathcal{T} , and the space of cumulative distribution function (CDF) of distributions in \mathcal{T} as \mathcal{P} .
 2. The dynamical system $\mathbf{x}(t) \in \mathcal{C}$, and the time derivative of $\mathbf{x}(t)$ have positive norm.
-

We consider that curves with different speed are the same and introduce an equivalence relation in \mathcal{C} .

DEFINITION A.2. $r_1 \in \mathcal{C} : [0, T_1] \rightarrow [0, 1]^d$, $r_2 \in \mathcal{C} : [0, T_2] \rightarrow [0, 1]^d$ are equivalent if there exists a C^1 strictly increasing map $s : [0, T_1] \rightarrow [0, T_2]$, such that $r_1 = r_2 \circ s$, which we denote as $r_1 \sim r_2$.

We remark that the s can be viewed as a change of velocity for the curve. The following lemma shows the existence of a representator with unit speed for each equivalence class

LEMMA A.3. For all $r \in \mathcal{C} : [0, T_1] \rightarrow [0, 1]^d$, there exists a unique C^1 strictly increasing map $s : [0, T_1] \rightarrow [0, T_2]$ such that $p = r \circ s$, $\|\frac{dp}{dt}(t)\|_2 \equiv 1$.

Proof. By Chain rule, $\frac{dp}{dt} = r' \circ s(t)s'(t)$, then we have

$$(A.1) \quad \left\| \frac{dp}{dt}(t) \right\|_2 = \|r' \circ s(t)\|_2 s'(t),$$

The desired s is obtained by solving the ODE for $[0, T_2]$

$$(A.2) \quad \begin{cases} s'(t) = \frac{1}{\|r' \circ s(t)\|} \\ s(0) = 0. \end{cases}$$

The global existence and uniqueness of s is guaranteed by the Existence and Uniqueness theorem for ODE. The regularity of s is given by the fact that $r \in C^1$. \square

LEMMA A.4. Let $r \in \mathcal{C} : [0, T] \rightarrow [0, 1]^d$ be an injective C^1 curve with $\|r'(t)\| \equiv 1$, then for any curve $\tilde{r} \in \mathcal{C} : [0, T_1] \rightarrow [0, 1]^d$ for some T_1 with $\|\tilde{r}'(t)\| \equiv 1$ such that $\tilde{r}(0) = r(0)$, $\{r(t) | t \in [0, T]\} = \{\tilde{r}(t) | t \in [0, T_1]\}$, $\tilde{r} \sim r$.

Proof. Suppose there exists such $\tilde{r}(t)$ that satisfies the aforementioned condition and is not equivalent to r .

First, it's easy to conclude that $T_1 = T$ by the arc length formula since $\|\tilde{r}'(t)\| \equiv \|r'(t)\| \equiv 1$.

Since $\tilde{r} \not\sim r$, there exists $t_0 \in (0, T]$, s.t. $r(t_0) \neq \tilde{r}(t_0)$. Consider the set $S = \{t \in [0, T] | r(t) \neq \tilde{r}(t)\}$, S is not empty and thus $t_1 := \inf(S) \in [0, T]$ exists. We claim that there exists $t_2 \neq t_1$, $r(t_2) = r(t_1)$, which leads to contradiction since r is injective.

Indeed, by $r(t_1) = \tilde{r}(t_1)$, we consider the extended curves from t_1 . Let $S_1^{\Delta t} = \{r(t_1 + t) | t \in (0, \Delta t]\}$, $S_2^{\Delta t} = \{\tilde{r}(t_1 + t) | t \in (0, \Delta t]\}$, we claim that there exists $\Delta t > 0$ such that $S_1^{\Delta t} \cap S_2^{\Delta t} = \emptyset$.

If our claim holds, then there exists $U \subset [0, T]$, such that $\{r(t) | t \in U\} = S_2^{\Delta t}$. We can find an series $\{\tilde{r}(\tilde{t}_i)\}_{i=1}^{+\infty}$ in $S_2^{\Delta t}$ converges to $\tilde{r}(t_1)$, thus the corresponding series

$\{r(\tilde{t}_i)\}_{i=1}^{+\infty}$ converges to $\tilde{r}(t_1)$ too. We then conclude that $\lim_{n \rightarrow \infty} \tilde{t}'_i = t_2 \neq t_1, r(t_2) = r(t_1)$ via a subsequence argument.

Now we proof the second claim, again we use proof by contradiction. Suppose for any $\Delta t > 0, S_1^{\Delta t} \cap S_2^{\Delta t} \neq \emptyset$, then $r(t)$ and $\tilde{r}(t)$ must coincide in $[t_1, t_1 + \Delta t_1]$ for small $\Delta t_1 > 0$ since $\|r'(t)\| \equiv \|\tilde{r}'(t)\| \equiv 1$ which contradicts to the fact that $t_1 = \inf\{t \in [0, 1] | r(t) \neq \tilde{r}(t)\}$. \square

Return to our setting, utilizing the lemma we prove the uniqueness theorem of our inverse problem

Proof. Given \mathbf{x}_{ob} and \mathbf{x}_0 , by theorem 2.1 we determine the dynamical system up to a strictly increasing coordinate transformation denoted by $[r(\cdot)]$, where $r(\cdot)$ is the smooth curve with unit speed

$$\begin{cases} \{r(t) | t \in [0, T_1]\} & = \text{Img}(\mathbf{x}_{ob}) \\ r(0) & = \mathbf{x}_0 \\ \|\frac{dr}{dt}\|_2 & = 1, \forall t \in [0, T] \end{cases},$$

where T_1 is the arclength of the trajectory in phase space and $\text{Img}(\mathbf{x}_{ob})$ is the range of \mathbf{x}_{ob} as a random vector. Thus $r^{-1}(\mathbf{x}_{ob})$ is a random variable with C^1 CDF $\tilde{P}(\cdot)$. The desire transformation is provided by its inverse explicitly

$$(A.3) \quad \begin{array}{ccc} \mathbf{x}^{-1} : \text{Img}(\mathbf{x}_{ob}) & \rightarrow & [0, T] \\ & \hat{\mathbf{x}} & \rightarrow P^{-1} \circ \tilde{P} \circ r^{-1}(\hat{\mathbf{x}}) \end{array},$$

by assumption the inverse map is C^1 and injective. \square

Appendix B. Restriction of FSNLS. To uncover the underlying dynamics from data without time labels, a straightforward approach involves utilizing a forward solver-based nonlinear least squares method with random collocations and a distributional metric. When applied to reconstructing dynamical systems from time-series data, the Forward Solver-based Nonlinear Least Squares (FSNLS) encounters certain challenges. It still faces these issues when it comes to learning distributions through trajectories. This section will delve into these issues through a series of illustrative experiments, employing the proposed algorithm 3.1.

Initially, we found that, in some relatively long trajectory, whether the success of the learning approach is profoundly susceptible to the preliminary selection of parameters owing to periodic or intricate structures present within the phase space. To illustrate this notion more comprehensively, we depict the loss landscape around the single trajectory of a simple ODEs:

$$\begin{cases} \frac{dx_1}{dt} = -0.1x_1^3 + 2x_2^3 \\ \frac{dx_2}{dt} = -2x_1^3 - 0.1x_2^3 \\ \mathbf{x}(0) = (4, 0)^\top. \end{cases}$$

where we observe the data with a uniform distribution $\mathbf{t} \sim \mathcal{U}(0, 10)$. Here we assume that the library is optimally determined as $\{x_1^3, x_2^3\}$ and the diagonal of the parameter matrix $A = \begin{bmatrix} -0.1 & A_{12} \\ A_{21} & -0.1 \end{bmatrix}$ is given. We estimate the Sliced Wasserstein Distance of trajectories with parameters in the neighbourhood of the ground truth $[1, 3] \times [-3, -1]$. As Fig 8(b) shows that the loss function manifests a strong non-convexity, resulting in even proximate selections would get stuck in local minima like the dashed blue curve in Fig 8(d) with improper learning rates. Nevertheless, the non-convexity can

be substantially alleviated for a uncomplicated trajectory. Fig8(c) exhibits a near-convex loss function in the identical parameter region for observation instances $t \in [0, 0.4]$. Such analysis suggest that partitioning intricate trajectory observations into abbreviated segments could diminish the complexity.

Another potential concern arises when the forward process, responsible for generating synthetic samples, may exhibit considerable stiffness or other numerical challenges, such as divergence. Implementing a more precise and stable numerical scheme could alleviate this issue; however, it may also incur a substantial computational expense and is inadequate to overcome innate divergence of systems with erroneous parameters. We plot the contour map of the $\sup_{t \in [0, 10]} \|\mathbf{x}_t\|_2$ in a large parameter space $\{(A_{12}, A_{21}) | (A_{12}, A_{21}) \in [-3, 3] \times [-3, 3]\}$ in 8(a), which shows that an initialization of parameters in the first or third quadrant results in blow up solution and prevent further update. The evolution of numerical ODE solver can be viewed as an auto-regressive model, which computational inefficient for long sequence rollout.

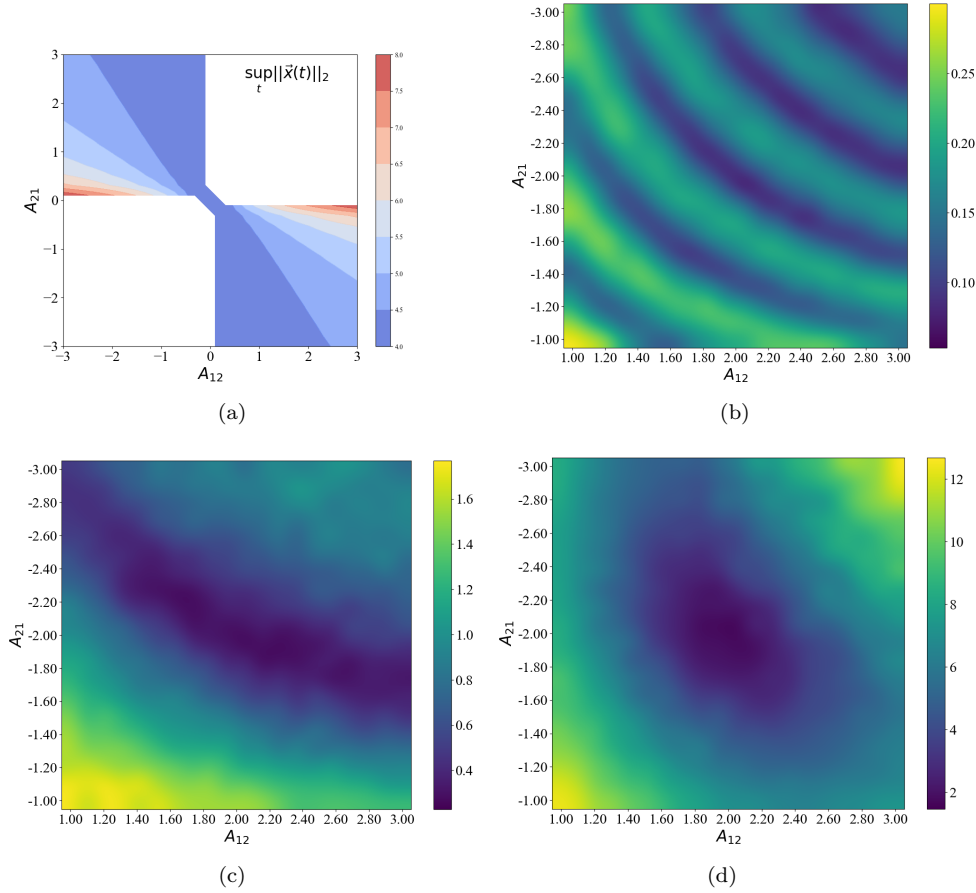


FIG. 8. Loss landscape analysis of Cubic2D problem: (a) The estimated $\sup_{t \in [0, 10]} \|\mathbf{x}_t\|_2$ of each parameter choice in $[-3, 3] \times [-3, 3]$; (b) The SWD loss landscape of A_{12}, A_{21} in $[1, 3] \times [-3, -1]$ with $T = 10$; (c) The SWD loss landscape of A_{12}, A_{21} in $[1, 3] \times [-3, -1]$ with $T = 0.4$; (d).

Appendix C. Experiment Detail.

Parameters	$n_{cluster}$	library	$\Lambda_{Threshold}$	lr	λ_{init}	λ_{reg}
Linear2D	10	Poly(3)+Exp	0.04	$3e-4$	0.5	$1e-3$
Cubic2D	10	Poly(3)+Exp	0.06	$6e-4$	0.5	$3e-5$
Linear3D	10	Poly(3)+Exp	0.04	$3e-4$	0.5	$1e-3$
Lorenz	10	Poly(3)+Exp	0.04	$3e-4$	0.5	$3e-5$
LV4D	10	Poly(2)+Exp	0.045	$6e-4$	0.5	$3e-4$
Duffing	10	Poly(3)+Exp	0.04	$3e-4$	0.5	$3e-4$
Pendulum	10	Poly(3)+sin+cos	0.04	$3e-4$	0.5	$3e-4$
Pendulum*	10	Poly(3)	0.02	$3e-4$	0.5	$3e-4$

TABLE 5

Implement parameters for illustrative examples. $n_{cluster}$ denotes the cluster number in the trajectory segmentation step, $Poly(n)$ represents the n -th order complete polynomials library in d -dimensional space (C_{p+d}^p elements), $\Lambda_{Threshold}$ is the threshold of filtering non-zero parameters in the parameter identification phase, λ_{init} and λ_{reg} is the weight of Initial Condition loss and Regularization loss in distribution matching phase.

Appendix D. STRidge Algorithm. Here we provide the details of the sequential thresholded ridge regression (STRidge) algorithm. In the STRidge method, each linear regression step retains the variables that were not sparsified in the previous regression. And if the original linear equation has n unknowns, the sparse regression operation is performed for a maximum of n iterations. STRidge will terminate directly if either of the following two conditions is met: 1) After a regression step, no additional variables are removed compared to the previous regression; 2) All variables have been removed. For further details of the STRidge algorithm, please refer to Algorithm D.1.

Algorithm D.1 STRidge Algorithm for Solving Linear System $A\mathbf{x} = \mathbf{b}$

Input: Coefficient matrix $A \in \mathbb{R}^{m \times n}$, vector $\mathbf{b} \in \mathbb{R}^m$, regular terms $\lambda > 0$, threshold $\eta > 0$

Compute x by ridge regression $x = \arg \min_w \|A\mathbf{w} - \mathbf{b}\|^2 + \lambda \|\mathbf{w}\|^2$, set $p = n$;

while True **do**

 Select index set $S^+ = \{x > \eta\}$, $S^- = \{x \leq \eta\}$;

if $\text{card}\{S^+\} = p$ **then**

 break

else

$p = \text{card}\{S^+\}$

end if

if $\text{card}\{S^+\} = 0$ **then**

 break

end if

$x[S^-] = 0, x[S^+] = \arg \min_w \|A[:, S^+]\mathbf{w} - \mathbf{b}[:, S^+]\|^2 + \lambda \|\mathbf{w}\|^2$

end while

if $S^+ \neq \emptyset$ **then**

$x[S^+] = \arg \min_w \|A[:, S^+]\mathbf{w} - \mathbf{b}[:, S^+]\|^2$

end if

return Vector $\mathbf{x} \in \mathbb{R}^n$ s.t. $A\mathbf{x} \approx \mathbf{b}$
